Binding Energies of Gas-Phase Metal Ions with Pyrrole: Experimental and Quantum Chemical Results

Alexei Gapeev, Chia-Ning Yang, Stephen J. Klippenstein, and Robert C. Dunbar*

Department of Chemistry, Case Western Reserve University, Cleveland, Ohio 44106

Received: July 27, 1999; In Final Form: December 1, 1999

Binding energies to pyrrole were determined for a number of main-group and transition-metal cations (both monomer complexes with one pyrrole ligand and dimer complexes with two ligands). Experimental data were obtained by radiative association kinetics measurements in the Fourier transform ion cyclotron resonance ion trapping mass spectrometer, along with ligand exchange equilibrium determinations (for the Mg^+ and Al^+ cases) using benzene as the reference ligand. Density functional calculations using the B3LYP hybrid functional were carried out on all complexes. The calculations indicated binding only to the π site of pyrrole, with no significantly stable binding site being found for binding of any metal ion in the vicinity of the nitrogen. Experimental binding energies for the transition-metal monomer complexes were parallel to previously reported benzene values. Mg^+ and Al^+ were more strongly bound to pyrrole than benzene, presumably due to the dipole moment of pyrrole. The quantum chemical binding energy values for the monomers were reasonably parallel to the experimental values, but were generally lower by a few kcal/mol. For the dimer complexes, the experimental and quantum chemical values were in satisfactory agreement. The pyrrole transition-metal dimers contrasted strongly with the trend previously reported for the corresponding benzene dimers, showing relatively weaker binding for the early transition metals falling to a minimum at Mn^+, rising sharply for the later transition metals, and dipping again for Cu^+.

Introduction

There has been an increasing interest in noncovalent intermolecular forces as important contributors to questions of structure and reactivity in organic,[1] organometallic,[2] and biological[3] systems. An example of particular interest to our group is the cation/aromatic-π-system interactions that play an important role in biological systems.[4] The thermochemistry of such interactions is central to understanding their behavior, so that the experimental measurement, quantum chemical calculation, and conceptual understanding of binding energies for cation/π interactions constitute timely and valuable targets.

Although metal cation/benzene interactions have been studied quite extensively, metal cation/heterocyclic aromatic interactions have received less attention, and few binding energy values are yet known for such compounds, among which nitrogen heterocycles in particular are of interest here. Among such systems, binding energies to pyrrole are interesting both because the pyrrole nucleus appears in various biomolecule contexts such as porphyrins and proteins and because this molecule has the highly unusual feature of a positively charged nitrogen atom region, making cation interaction with the heteroatom binding site unfavorable. Typically the nitrogen atom site in a nitrogen heterocycle is dominant for binding cations, but this exceptional characteristic of pyrrole results in the π binding site being at least as favorable as any nitrogen site with respect to cation binding. The relative favorablility of π-site binding versus N-site binding is also reflected in indole, where both π sites are believed to be more favorable than the N site.[4−8]

The analysis of radiative association (RA) kinetics for the reaction

$$M^+ + L \rightarrow ML^+ \qquad (1)$$

is becoming a productive method for determination of binding energies in gas-phase species. This approach has been applied at different degrees of sophistication: The simple generic "standard hydrocarbon" (StH) model[9] is an easily implemented semiquantitative approach, while full-scale variational transition-state (VTST) modeling based on ab initio calculations[10] is a fully quantitative and accurate approach, within the assumptions that transition-state theory gives a valid description of the association kinetics and that the radiative stabilization process is correctly modeled.

Ligand exchange equilibrium

$$ML_1^+ + L_2 \rightleftharpoons ML_2^+ + L_1 \qquad (2)$$

offers another frequently useful way of determining binding energies. (See ref 11 for one example of the innumerable applications of this approach.) Unfortunately, for most of the systems of interest here the efficient addition of a second ligand to the ML^+ complex, dominating over ligand exchange, precluded the use of exchange equilibrium as a quantitative thermochemical approach. However, Mg^+ and Al^+, which do not form dimer complexes under these conditions, are not subject to this problem, and it was possible to make equilibrium measurements to compare their binding energies with pyrrole versus benzene. This provides a valuable cross check on the accuracy of the RA kinetics approach for the pyrrole complexes.

The focus of the present study was on the cationic pyrrole complexes with the first transition-metal row as well as Mg, Al, Mo, and W. Of interest is the sequence of association reactions

* To whom correspondence should be addressed.

10.1021/jp992627d CCC: $19.00
Published on Web 03/18/2000

$$M^+ + Py \rightarrow MPy^+ \quad (3)$$

$$MPy^+ + Py \rightarrow MPy_2^+ \quad (4)$$

where Py is pyrrole.

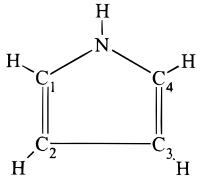

Pyrrole

In this paper we assign "experimental" values to the binding energies described by reactions 3 and 4, using RA kinetic modeling of experimental kinetic data, in which B3LYP−density functional theory (DFT) quantum chemical calculations are used to provide vibrational frequencies and IR intensities of the metastable complex. Independent of this approach, the same B3LYP−DFT calculations are also used to provide purely theoretical structures and binding energy values. Finally, ligand exchange equilibria versus benzene are used where possible to reconfirm the experimental binding energies.

Methods

Instrumental Details. All experiments were performed on a modified Nicolet FTMS-2000 spectrometer with a 3 T superconducting magnet, 10 × 5 × 5 cm cell, and IonSpec data system (more fully described in ref 12). The vacuum chamber was pumped by a 1000 L/s Asti-Cryogenics cryopump on the low-pressure side and a 100 L/s Alcatel diffusion pump on the high-pressure side (the cell being placed on the low-pressure side of the vacuum system adjacent to the conductance limit plate). This dual pumping system yields a background pressure below 5×10^{-10} Torr in the low-pressure region.

Pressures were measured with an ionization gauge. Although the gauge pressure of pyrrole was corrected by the known ionization gauge factor,[13] the pressure in the cell was higher than at the gauge. Calibration of the instrument with reference reactions indicates that the cell pressure is higher than that at the ion gauge by a factor of 3.0 ± 0.5. After correction for this, the absolute pyrrole pressure was considered to be uncertain by less than a factor of 2. The error bars given below for the derived binding energies are based on a cumulative uncertainty of a factor of 2 in the radiative association rate constants (except for a few cases which are noted). Relative rate constant comparisons within this study are both more confident and more accurate than the absolute rate constant values.

Pyrrole was purchased from Aldrich Inc. in 98% purity. It was vacuum distilled, and subjected to multiple freeze−pump−thaw cycles to remove dissolved gases. Pyrrole was introduced into the high-vacuum chamber through a Varian leak valve located on the high-pressure side of the vacuum system. For most metal ions the pyrrole pressure was in the range $(2-9) \times 10^{-8}$ Torr. However, for Mn^+ the slowness of the dimer formation reaction made it desirable to go up to 4.5×10^{-7} Torr. The likelihood of a significant collisional component of the association kinetics for this case is addressed below.

The precursor metal ions were generated by a pulsed Nd:YAG laser (532 nm) focused on a metal target mounted on the solid probe tip. Thermalization of ions was achieved through collisions with pyrrole or with inert gas (argon) followed by isolation of ions of interest. The intensities of the metal ion and the corresponding complexes were monitored as a function of reaction time to derive the association rate constant. Rate constants were derived by fitting to the kinetic scheme of reactions 3 and 4, including competing side reactions when these were present. Figure 1 shows an illustrative series of spectra.

Equilibrium Ligand Exchange Experiments. The equilibrium measurements were done using the same experimental setup. Simultaneous measurement of ion intensities that differ by more then 2 orders of magnitude cannot be done reliably with this instrument. The binding energy difference between benzene and pyrrole is large for an equilibrium experiment, and to stay within this constraint on the peak ratios, it was necessary to use a high ratio of neutral-reagent pressures. In fact benzene/pyrrole pressure ratios on the order of 1000:1 were used. The pyrrole pressure, typically 1×10^{-9} Torr, was determined by observing the rate of the proton-transfer reaction from CH_5^+, which was in turn calibrated at higher pressures where the ion gauge measurement was more reliable. For benzene, typically at 2×10^{-6} Torr, ionization gauge readings were used with appropriate corrections.

Quantum Chemistry. Nonlocal DFT was employed in the determination of the optimized structures, binding energies, vibrational frequencies, and infrared absorption intensities for each of the metal/pyrrole monomer and dimer cations. These determinations employed the B3-LYP (Becke-3 Lee−Yang−Parr) hybrid functional.[14] Three basis sets were employed in these determinations. The smallest basis set (B1) consisted of the 6-311G basis for the metal ions, and the 3-21G basis for the C, N, and H atoms.[15] This basis set was employed in the determination of the optimized structures and vibrational frequencies for the dimer cations. The second basis set (B2), consisting of the 6-311+G* basis for the metal ions, and the 6-31G* basis for the C, N, and H atoms,[15] was employed in the geometrical optimization and vibrational analysis for the monomers. The addition of diffuse functions for the C and N atoms (6-31+G*) to B2 provided a third basis set (B3) which was employed in the determination of improved estimates for the binding energies of both the monomer and dimer species.

For the monomers, the basis set superposition error (BSSE) for the B3 basis was estimated according to a recently described scheme of Xantheas,[16] and was found to lie between 0.5 and 1.4 kcal/mol. The binding energies reported here include this BSSE correction for the monomers and a constant BSSE correction of 1.0 kcal/mol for the dimers. Variations in the zero-point energy are also incorporated in these binding energy estimates.

As with many other quantum chemical methods, the B3LYP−density functional theory does not provide especially accurate estimates of the electronic excitation energies of the free metal ions. Thus, for reactions involving transitions in the spin of the metal ion, it is generally more meaningful to estimate the ground-state to ground-state binding energy by combining the theoretical estimate of the spin-conserving dissociation energy with the experimental energy[17] for the spin-transition process in the free metal ion.[18,19] This procedure was followed in obtaining the present theoretical estimates for the binding energies for the Fe and Ti monomer complexes. The formation of the Mn dimer complex also involves a spin change from a septet to a quintet. However, in this instance there is no available experimental value for the septet to quintet transition of the dissociated species ($MnPy^+$), so this procedure could not be

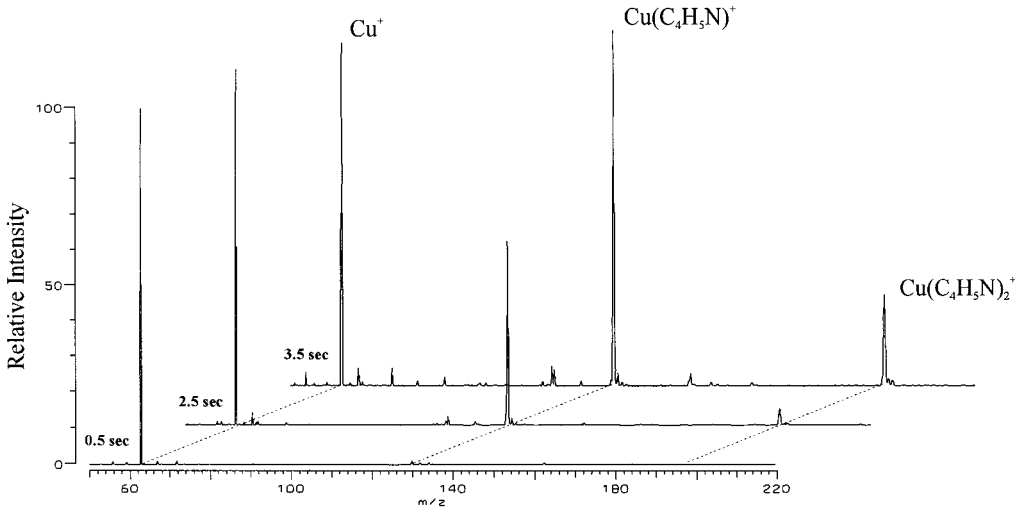

Figure 1. Illustrative spectra showing the sequential formation of copper complexes with one and two pyrrole molecules. Pyrrole pressure 2.7×10^{-8} Torr.

followed; accordingly for this case the binding energy was calculated directly for the ground-state to ground-state dissociation.

For comparison purposes the binding energies of the metal/benzene cations have been reevaluated with an equivalent theoretical approach.[20] All of the quantum chemical calculations reported here were performed with the GAUSSIAN94 software.[15]

Kinetic Modeling. RA kinetics have been discussed in detail elsewhere.[10,21−25] In a radiative association reaction two gas-phase species cluster together, forming a product molecule with photon(s) being emitted. A collision between the ion A^+ and the molecule B gives a metastable ion−molecule complex $(AB)^{+}$*. This complex has too much internal energy to be stable. The stabilization of AB^{+}* occurs either through a collision with a third body (M) or through emission of a photon:

$$A^+ + B \underset{k_b}{\overset{k_f}{\rightleftharpoons}} (AB)^{+*} \xrightarrow{k_r} AB^+ \qquad (AB)^{+*} \xrightarrow[k_c\beta]{[M]} AB^+ \qquad (5)$$

These stabilization pathways compete with redissociation of AB^{+}* back to the reactants.

For reaction conditions where the pressure is low (usually less than 10^{-6} Torr), radiative stabilization (k_r) may become substantial. In the low-pressure limit where radiative stabilization dominates over collisional stabilization, the process becomes that of radiative association, and the apparent bimolecular rate constant k_2 for association becomes the true bimolecular rate constant k_{RA}. The strong dependence of k_{RA} on the binding energy makes the analysis of observed rate constants a useful route to determining association thermochemistry.

We applied two approaches to analyzing the kinetic data to obtain binding energy values: (i) VTST modeling with quantum chemical evaluation of the molecular parameters and (ii) the StH semiquantitative estimation method based on generic modeling of typical properties of ions and neutrals.[9]

VTST modeling has been shown to provide accurate results in predicting the kinetics of a variety of RA reactions.[9,10,23,26−28] The details of the theory have been described thoroughly previously.[10] There are two major parts involved.

The first part is the calculation of the photon emission rate (k_r) from the metastable complex. For a molecule considered as a set of weakly coupled harmonic oscillators, this is given by

$$k_r\,(s^{-1}) = \sum_{n=1}^{N}\sum_{i=1}^{N}(1.25 \times 10^{-7}) n P_i(n)\, I_i(n)\, \nu^2 \qquad (6)$$

where N is the number of vibrational modes, $P_i(n)$ is the probability for normal mode i to be at level n, I_i (km mol^{-1}) is the IR absorption intensity for the $0 \rightarrow 1$ transition of mode i, and ν_i (cm^{-1}) is the vibrational frequency for this mode. The probability $P_i(n)$ is calculated statistically by a state-counting algorithm.

The second part of the k_{RA} modeling is the formation and redissociation kinetics of the metastable complex AB^{+}*. The kinetics are treated by a VTST approach incorporating convolutions over a thermal distribution of energies and angular momenta for the reactants and over the distribution of angular momenta and energies of the complex. The expression for k_2 is the following:

$$k_2 = \frac{1}{hQ_{\text{reactants}}}\int\int dE\, dJ\, N_{EJ} e^{-E/kT} \left\{\frac{k_r(E,J) + k_c(E,J)[M]}{k_b(E,J) + k_r(E,J) + k_c(E,J)[M]}\right\} \qquad (7)$$

where $Q_{\text{reactants}}$ is the canonical partition function for separated reactants, N_{EJ} is the cumulative reaction probability (or number-of-states function) of the complex, [M] is the neutral bath gas pressure, and k_c is the rate constant for collisional stabilization. The binding energy of the complex is implicitly contained in the right-hand side of eq 7, since the redissociation rate constant $k_b(E,J)$ is a strong function of binding energy. The optimized geometries and vibrational frequencies of the reactants are needed to calculate $Q_{\text{reactants}}$. These parameters, along with IR frequencies and intensities of the complex AB^+, are taken from the B3LYP−DFT calculations, and form the input for a Fortran-based program (VariFlex[29]), which calculates the association rate constant k_2 corresponding to an assumed binding energy value of ion A^+ with neutral B.

For the dimers the lowest frequency vibrational mode corresponds to an internal rotation of one of the pyrrole ligands relative to the other. In the kinetic modeling we considered both free rotor and harmonic vibration treatments for this mode. The former is probably more appropriate given the weakness of the

hindering potential as evidenced by the smallness of the harmonic vibrational frequency.

For a number of associations, the lowest electronic spin state of the complex differs from that of the reactants. Furthermore, there are also many instances where a thermal distribution of the reactant metal ions would have a significant population in a number of different spin−orbit states. For these cases, an accurate treatment of the kinetics requires some knowledge of the rates of transition among the different electronic states, and of the energetic separation between these states along the reaction path. In this work, in keeping with the statistical assumptions for the kinetics, it was assumed that the electronic transitions are rapid and a statistical distribution of electronic states is maintained throughout. Furthermore, it was assumed that the electronic separations in the transition-state region are equivalent to those of the free metal ions. While these assumptions may not always be valid, they do at least allow for a quite meaningful first estimate for the kinetics.

The accessibility of multiple electronic states in the complex provides various complications to the modeling. One aspect that can be easily addressed is their contribution to the density of states. The results presented in Tables 5 and 6 include a contribution calculated under the assumption that the vibrational frequencies and rotational constants of the excited electronic states are equal to those of the ground electronic state. Neglecting the contribution from the excited electronic states yields modeled binding energies which are 0.4, 0.4, 3.2, 1.4, and 0.9 kcal/mol lower for the Ti/pyrrole, V/pyrrole, Fe/pyrrole, Co/pyrrole, and Ni/pyrrole monomer cations, respectively. Uncertainties in the populations and transitions among the electronic states of the free ions provide similar levels of uncertainty in the modeling of the monomer association rates. It is worth noting that these modeling uncertainties are largely absent for the Mg, Al, Cr, Mn, Cu, Mo, and W species, for which no kinetically significant excited electronic states are likely.

For the dimers the excited electronic states of the complex are much less significant. For each metal their neglect decreases the modeled binding energy by 0.1 kcal/mol or less. The energetics of the electronically excited states of the monomers might also be expected to play a role in the modeling of the kinetics for the dimer formation. However, for a thermal distribution at 300 K there is very little population of excited electronic states in the monomers. Thus, for the dimer modeling, there is comparatively little uncertainty arising from excited electronic states.

For the monomer species the radiative rate constant (IR photon emission rate) for complexes having internal energy equal to the dissociation threshold was typically calculated to be about 40 s^{-1}. For the dimer species it was instead about 20 s^{-1}.

The pyrrole pressures used in these experiments were not low enough to dismiss the possibility of some contribution of three-body collisional association to the observed kinetics, and the VariFlex package was used to make estimates and apply corrections to the binding energy assignments to account for this effect. Although the collisional association process was not characterized in enough detail for us to have great confidence in its modeling, the corrections to the present results are mostly so small that the detailed accuracy of this aspect of the modeling is not important. VariFlex modeling was used to calculate collisional association contributions, using dipole-corrected Langevin collision rates[29] and making the strong-collision assumption (every collision of a metastable ion−neutral complex with a neutral pyrrole molecule results in a stabilized complex.) At the pressures used for most experiments ($<1 \times 10^{-7}$ Torr), VariFlex modeling indicated that the contribution of collisional stabilization to the association rate constant was less than about 10%, and the corresponding effect on the binding energy assignments (on the order of 0.5 kcal mol^{-1}) was within experimental error. However, for Mn^+ the use of a high neutral pressure (4.5×10^{-7} Torr) meant that the association kinetics were about 50% collisional, and the binding energy assigned from VTST modeling was strongly affected by the three-body collisional kinetics modeled by the VariFlex package. The uncertainty in this case was assigned somewhat more conservatively than for the other systems.

TABLE 1: B3LYP Structures and Energetics of Metal/Pyrrole Cations

metal	state	R_{M-ring}[a] (Å)	Δx[b] (Å)	ΔZ_N[c] (Å)	D_o[d] (kcal/mol)	ΔD_{benz}[e] (kcal/mol)
Na	$^1A'$	2.416 (2.376)	0.69	0.021	25.8	3.0
Mg	$^2A'$	2.328 (2.294)	0.51	0.006	36.0	6.1
Al	$^1A'$	2.357 (2.399)	0.82	0.006	35.7	6.4
Ti	$^4A''$	2.017 (1.883)	1.04	0.004	48.9	−5.5
V	$^5A''$	2.135 (1.929)	0.64	−0.069	49.4	1.9
Cr	$^6A'$	2.246 (2.104)	−0.11	−0.009	41.4	5.2
Mn	$^7A'$	2.380 (2.360)	0.55	0.006	37.4	6.2
Fe	^4A	2.010 (1.665)	0.47	−0.011	49.1	−0.6
Co	$^3A''$	1.912 (1.663)	0.77	−0.022	54.8	−4.1
Ni	^2A	1.975 (1.715)	0.15	−0.046	61.0	3.8
Cu	$^1A'$	1.986 (1.848)	−0.33	−0.009	58.3	9.0
Mo	$^6A'$	2.347	−0.34	−0.007	38.6	
W	$^6A'$	2.201	−0.45	0.004	58.8	

[a] Distance from the metal M to the CCCC plane (see Scheme 1). The primary entry is the value for the metal/pyrrole cation while that in parentheses is for the metal/benzene cation. For comparison purposes the Fe and Ni geometrical parameters reported here are for the optimum C_s geometry rather than the slightly lower energy C_1 geometry. [b] Offset distance of the metal from the edge of the ring (see Scheme 1). More positive values correspond to the metal being closer to N, while a negative value means the metal lies outside the perimeter of the ring. [c] Out-of-plane displacement of the N atom relative to the CCCC plane. A positive value implies displacement toward the metal atom. [d] Zero-point and BSSE-corrected binding energy for the metal/pyrrole cations. [e] The DFT binding energy of the metal/pyrrole cation relative to that of the metal/benzene cation [$D_e(M(C_4H_5N)^+ - D_e(M(C_6H_6)^+)$], from comparison with DFT calculations for benzene complexes.[20]

Results

Quantum Chemical Results. *Monomers.* The structures and binding energies obtained from the present B3LYP−density functional theory calculations for the metal/pyrrole cations are summarized in Table 1, and displayed graphically in Figure 2. (Scheme 1 defines the geometrical parameters given in the table.) The corresponding metal−ligand vibrational frequencies and rotational constants are reported in Table 2. The remaining vibrational frequencies not tabulated are quite similar to those for the free pyrrole species. The average spin squared was within 0.03 of the pure spin state value for each of the states reported in these tables, which suggests that any spin contamination is insignificant.

For the Na, Mg, Al, and Mn monomers the bond lengths are quite similar to those for the corresponding metal/benzene cations, being only 0.03 Å greater on average. For these four complexes the metal ion lies essentially directly above the center of the four-carbon ring portion of the ligand (see Scheme 1). These increased bond lengths may be indicative of the smaller size of the pyrrole ring as compared to the benzene ring. For these same four species the binding energy is greater, by 5 kcal/

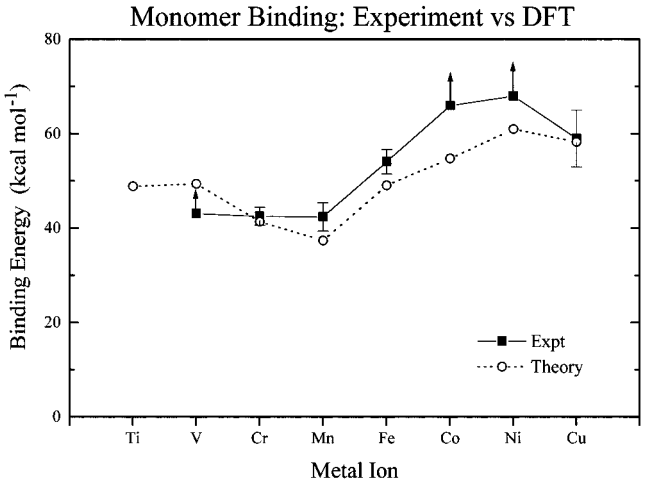

Figure 2. Comparison of experimental binding energies from RA kinetics analysis with quantum chemical values from B3LYP−DFT calculations. Note that the experimental value for V^+ is a lower limit because of competing reaction complications, and the actual value is definitely higher than shown. The Co^+ and Ni^+ points are also lower limits because of saturation, and the actual values may be higher.

SCHEME 1

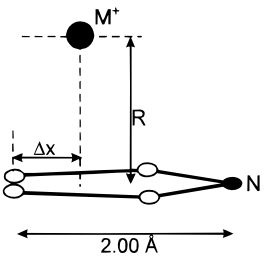

TABLE 2: Metal−Ligand Vibrational Frequencies and Rotational Constants for Metal/Pyrrole Cations

metal	state	vibrational frequencies (cm^{-1})	rotational constants (cm^{-1})
Na	$^1A'$	99, 138, 238	0.152, 0.107, 0.106
Mg	$^2A'$	100, 134, 277	0.156, 0.108, 0.105
Al	$^1A'$	147, 172, 247	0.150, 0.103, 0.103
Ti	$^4A''$	274, 281, 295	0.148, 0.098, 0.098
V	$^5A''$	152, 168, 293	0.154, 0.086, 0.085
Cr	$^6A'$	74, 88, 272	0.170, 0.070, 0.067
Mn	$^7A'$	91, 128, 215	0.153, 0.072, 0.072
Fe	^4A	81, 109, 288	0.157, 0.089, 0.087
Co	$^3A''$	66, 88, 283	0.150, 0.096, 0.096
Ni	^2A	46, 107, 330	0.168, 0.083, 0.078
Cu	$^1A'$	56, 124, 310	0.182, 0.070, 0.064
Mo	$^6A'$	62, 103, 242	0.173, 0.062, 0.056
W	$^6A'$	112, 121, 266	0.177, 0.042, 0.041

mol on average, than that for the corresponding metal/benzene cations, indicating a more favorable ion−ligand interaction for the pyrrole ligand.

For the remaining monomers the increase in the metal−pyrrole bond length (relative to the metal−benzene bond length) is much greater, ranging from 0.13 to 0.35 Å. For Ti, Fe, and Co, the greater bond lengths correspond to a reduction in the binding energies for the pyrrole complexes, while for V the pyrrole binding energy is greater, but only by 2 kcal/mol. The metal in each of these four complexes again lies more or less above the center of the four-carbon ring portion of the pyrrole ligand. For Cr, Ni, and Cu, the metal/pyrrole binding energies are substantially greater than the corresponding metal/benzene binding energies (by 4−9 kcal/mol), but now there is a significant change in the geometry. In particular, the metal has now shifted away from the N to the opposite side of the ring. For the Cr and Cu species the metals actually lie outside the perimeter of the ring.

A number of other electronic states of the monomers were also studied to verify the configuration of the ground state and also to provide further information for the kinetic modeling. In particular, estimated electronic excitation energies allow for an estimate of their contribution to the density of states for the complex. For Na, Mg, Al, and Cu there are not expected to be any low-lying electronic states. For Cr we examined both quartet and doublet spin states with a d^5 configuration and found the lowest excited state to be a $^4A'$ state lying 35 kcal/mol higher in energy. Mo and W should be similar to Cr. The lowest excited state for Mn appears to be a $^5A'$ state with a mixture of d^5s and d^6 configurations, which lies 9 kcal/mol higher in energy. However, this state has a significant spin contamination ($\langle S^2 \rangle = 6.53$). A $^5A''$ state was also found which is 14 kcal/mol above the ground state. The latter state has a d^6 configuration and negligible spin contamination. It is not expected that any of these states would have a significant effect on the kinetics. The absence of any low-lying electronic states for both the free metal ions and the monomer complexes should make the kinetic modeling for these metals much more secure than for the remaining ones.

For the remaining metals the d orbitals are partially filled in the monomer complexes, which leads to near degeneracies for different occupations and multiple electronic states having the same spin. In each case the ground-state configuration corresponds closely to that for the metal/benzene cations, where the d_{xy} and $d_{x^2-y^2}$ orbitals are occupied first, followed by the d_{z^2}, and then the d_{xz} and d_{yz} orbitals, where the z axis is the metal−ligand axis. For the metal/pyrroles, defining the x axis as the C_2 symmetry axis of pyrrole implies that the $d_{x^2-y^2}$, d_{z^2}, and d_{xz} orbitals mix together and transform as A′ orbitals while the d_{xy} and d_{yz} orbitals mix together and transform as A″ orbitals.

For Ti the ground state is a $^4A''$ state with metal orbital configuration (A'^2A'') and the first excited state appears to be a $^4A'$ state (A'^3) which lies 8 kcal/mol higher. Various other quartet states have similar spacings from this first excited state, and the lowest doublet states are also higher in energy than this. For V, the ground state is a $^5A''$ state (A'^3A'') and the first excited state is a $^5A'$ state ($A'^3A''^2$) which lies 5 kcal/mol higher. Again, other quintet, triplet, and singlet states would be expected to be substantially higher in energy.

For Fe, in C_s symmetry, the ground state is a $^4A''$ state ($A'^4A''^3$) but the $^4A'$ state ($A'^5A''^2$) is only 1.7 kcal/mol higher. This near degeneracy results in a reduction of symmetry to C_1 symmetry where the two states can mix. The calculated energy lowering for the symmetry reduction is very small (<0.1 kcal/mol), and thus the first excited state should still lie only about 1.7 kcal/mol higher. The lowest sextet states [$^6A''(dA'^3dA''^3sA')$] and [$^6A'(dA'^4dA''^2sA')$] are estimated to lie only 2.3 and 2.7 kcal/mol higher, respectively (after correcting for the errors in the B3LYP estimates for the excitation energies in the free metal ion).

For Co, the ground state is a $^3A''$ state ($A'^5A''^3$) and the first excited state is a $^3A'$ state ($A'^4A''^4$) which lies only 2.0 kcal/mol higher. Additional triplet states should be somewhat higher in energy (e.g., 10 kcal/mol higher) while the lowest singlet state $^1A'$ ($A'^6A''^2$) is much higher in energy (47.0 kcal/mol). For Ni, in C_s symmetry, the ground state is a $^2A''$ state with a hole in the A″ d orbital while the $^2A'$ state is 4.4 kcal/mol higher. The near degeneracy of these two states again leads to a

TABLE 3: B3LYP Structures and Energetics of Metal/Pyrrole Dimer Cations

metal	state	R_{M-ring}[a] (Å)	Δx[b] (Å)	D_o[c] (kcal/mol)
Na	$^1A(C_2)$	2.381	0.81	19.6
Mg	$^2A(C_2)$	2.548	0.58	18.7
Al	$^1A(C_2)$	2.637	0.99	15.6
Ti	$^4B(C_2)$	2.056	1.05	45.4
V	$^5B_g(C_{2h})$	2.157	0.50	37.6
Cr	$^6A_g(C_{2h})$	2.217	−0.22	31.5
Mn	$^5A(C_2)$	2.171	−0.23	29.9
Fe	$^4A(C_2)$	2.010	−0.34	39.7
Co	$^3B_g(C_{2h})$	2.028	−0.04	39.6
Ni	$^2B(C_2)$	1.976	−0.06	43.7
Cu	$^1A_g(C_{2h})$	1.945	−0.37	38.7

[a] Distance from the metal M to the CCCC plane (see Scheme 2). In each case the structural parameters are for the optimum C_{2h} geometry. [b] Distance of the metal offset from the edge of the ring (see Scheme 2). More positive values correspond to the metal being closer to N, while negative values mean the metal lies outside the perimeter of the ring. [c] Zero-point and BSSE-corrected binding energy for the metal/pyrrole dimer cations.

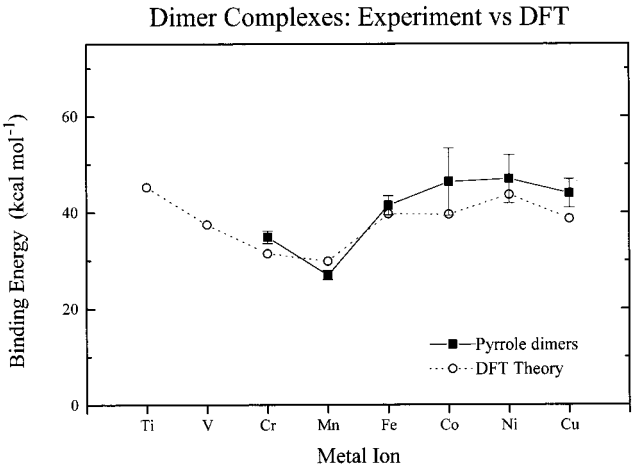

Figure 3. Comparison of experimental binding energies for the dimer complexes from RA kinetics analysis (VTST method) with quantum chemical values from B3LYP−DFT calculations.

reduction to C_1 symmetry with less than a 0.1 kcal/mol reduction in the energy.

It is interesting to consider also the possibility that the metals might bind to the p_z orbital of the N rather than to the π system as a whole. To investigate this possibility, we have performed restricted optimizations for the Na, Cr, Co, Ni, and Cu monomer complexes. In these optimizations the CCCC framework was restricted to be planar and the MNX angle (where X is the midpoint of the line joining the two central C atoms) was held fixed at various values. Examination of the potential and its gradient for MNX angles near tetrahedral-nitrogen values indicated the presence or absence of a local minimum in the potential in this region. With the B1 basis local minima were located for Cr, Ni, Co, and Cu; these minima were generally about 10 kcal/mol higher than the global minima. For these local minima the N was effectively tetrahedral with the H bent away from the metal atom. However, for all but Cu, these minima disappeared upon proceeding to the B2 basis, and even for Cu it was unclear whether the minimum still existed at this level. Thus, while there are some indications of covalent interactions between the metal and N for tetrahedral geometries, these interactions are not strong enough to counteract the electrostatic inhibition arising from the accumulation of positive charge in the nitrogen region.

A further possibility for binding is offered by the existence of two less stable tautomers of pyrrole (the pyrrolenine structures) in which the *N*-hydrogen is shifted to one of the carbons.[31] These structures open a free binding site for the metal ion on the nitrogen atom, and could potentially give more stable metal complex ions. In particular, the higher than expected binding energies derived from experiment for the monomer complexes of Co^+, Ni^+, Mo^+, and W^+ might be rationalized by rearrangement of the π complex to the metal/pyrrolenine structure. This possibility was tested computationally for the Ni^+ complex. The metal/pyrrolenine structures were found to have stable potential minima of reasonable energies. However, no geometry of the complex could be found having greater stability than the corresponding unrearranged metal/pyrrole π complex. The most stable isomeric structures found were at least 2 kcal mol^{-1} less stable than the pyrrole π complex.

Dimers. The B3LYP-estimated structures and binding energies for the metal/pyrrole dimer cations are summarized in Table 3 and Figure 3, and the corresponding metal−ligand vibrational frequencies and rotational constants are reported in Table 4. (Scheme 2 defines the geometrical parameters for these complexes.) The remaining vibrational frequencies are again similar to those for the free pyrrole species. The average spin squared was again within 0.03 of the pure spin state value for each of the states except the ^5A state of Mn, where the difference was only moderately larger, i.e., 0.06.

Sandwich structures, with the metal between the two pyrrole ligands, were assumed for each of the metals (Scheme 2). Vibrational analyses indicate that at the B3LYP/B1 level local minima exist for either C_{2h} or C_2 symmetry for each case. (That is, the rings may be oriented with opposed nitrogens as in Scheme 2 (C_{2h}) or with staggered nitrogens (C_2, not illustrated).) For Na, Ti, and Ni, the C_2 optimized structures differ by less than 0.3 kcal/mol from the corresponding optimized structures in C_{2h} symmetry. For Mg, Al, Mn, and Fe, the C_{2h} to C_2 relaxation energy is much greater, being 7.3, 3.9, 5.4, and 3.7 kcal/mol, respectively. The Δx values (Table 3) indicate that the metal prefers to lie outside the pyrrole rings (on the C side) for all the transition metals beyond Cr, while the Na, Mg, Ti, V, and Al cations are roughly in the center of the pyrrole rings. For these dimer species no attempt was made to locate structures involving the binding of the metal to a N site.

Various alternative electronic states were also investigated for some of these dimer species. Again no low-lying excited electronic states are expected for the Na, Mg, Al, and Cu species. For Cr, ^2B_g and ^4B_g states were found with excitation energies of 23 and 26 kcal/mol, respectively. For Mn, ^1A, ^7A_g, and ^3B_g states were found at excitation energies of 17, 19, and 32 kcal/mol. Furthermore, in C_{2h} symmetry the ^5A_g and ^5B_g states lie 5.4 and 7.6 kcal/mol higher than the ground state. The ^5A_g state correlates with the ground ^5A state in C_2 symmetry while the ^5B_g state correlates with an excited state.

For Fe, in C_{2h} symmetry, the ^4B_g and ^4A_g states lie 3.7 and 5.9 kcal/mol higher than the ground state, with one state correlating with the ground ^4A state and the other correlating with a first excited state in C_2 symmetry. For Co, the first excited states should correspond to different triplet configurations while the ground singlet state lies 22 kcal/mol higher. For Ni, in C_{2h} symmetry, the ^2B_g and ^2A_g states lie 0.3 and 7.6 kcal/mol higher than the ground state, with the ^2B_g state correlating with the ground state while the ^2A_g correlates with the first excited state.

Experimental Results

Reactivity Patterns. Under these conditions pyrrole was found to react with members of the first transition-metal row

TABLE 4: Metal−Ligand Vibrational Frequencies and Rotational Constants for Metal/Pyrrole Dimer Cations

metal	state	vibrational frequencies (cm^{-1})	rotational constants (cm^{-1})
Na	$^1A(C_2)$	20, 37, 39, 83, 119, 136, 140, 170, 307	0.0743, 0.0192, 0.0192
Mg	$^2A(C_2)$	23, 45, 71, 84, 95, 115, 117, 240, 252	0.0832, 0.0181, 0.0177
Al	$^1A(C_2)$	27, 40, 58, 89, 127, 131, 140, 202, 215	0.0777, 0.0179, 0.0178
Ti	$^4B(C_2)$	51, 90, 94, 219, 249, 253, 335, 360, 370	0.0730, 0.0250, 0.0250
V	$^5B_g(C_{2h})$	27, 70, 72, 111, 157, 161, 178, 267, 333	0.0761, 0.0218, 0.0217
Cr	$^6A_g(C_{2h})$	16, 50, 57, 85, 107, 121, 134, 243, 328	0.0848, 0.0172, 0.0168
Mn	$^5A(C_2)$	15, 66, 67, 96, 109, 155, 181, 300, 314	0.0803, 0.0184, 0.0176
Fe	$^4A(C_2)$	26, 56, 62, 67, 87, 156, 183, 307, 330	0.0864, 0.0185, 0.0178
Co	$^3B_g(C_{2h})$	46, 56, 62, 64, 95, 98, 189, 298, 373	0.0837, 0.0206, 0.0200
Ni	$^2B(C_2)$	42, 49, 75, 78, 86, 134, 186, 311, 380	0.0842, 0.0213, 0.0206
Cu	^1A_g	18, 27, 64, 92, 103, 131, 175, 299, 371	0.0897, 0.0192, 0.0184

SCHEME 2

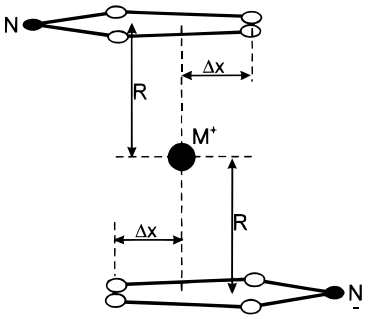

(Ti^+−Cu^+) as well as with Al^+, Mg^+, Mo^+, and W^+. The radiative association pathway (eq 3) dominates for Mg^+, Al^+, the later first-row transition-metal ions (Cr^+−Cu^+), and Mo^+. For Ti^+, V^+, and W^+, the kinetics were complicated by major competition from other reaction channels.

The major route for the Ti^+/Py system is nitrogen extraction by Ti^+ from a pyrrole molecule, yielding $C_4H_5^+$. This cation reacts further with another pyrrole molecule, forming an adduct, so the observed reaction scheme is

$$Ti^+ + C_4H_5N \rightarrow TiC_4H_5N^+ \quad (8)$$

$$\rightarrow C_4H_5^+ + TiN \quad (9)$$

$$C_4H_5^+ + C_4H_5N \rightarrow C_8H_{10}N^+ \quad (10)$$

Ti^+/pyrrole monomer complex formation, eq 8, was observed only when there was $\sim 4 \times 10^{-6}$ Torr of nitrogen as a bath gas for ion cooling. Under such conditions of extensive reactant-ion thermalization, we estimate the branching ratio between the RA pathway (eq 8) and ion−molecule reaction (eq 9) in this system as 1:10. The observation of this small amount of complex formation (eq 8) gives a lower limit on the association rate that would be observed in the absence of the competing elimination reaction channel, but without actually modeling the competition between these two channels, as well as the contribution of collisional stabilization to the association channel, it is not possible to assign an accurate binding energy. We can only say that the binding energy must be quite large (on the order of 50 kcal mol^{-1} or more) to account for the observed extent of association complex formation.

In the vanadium/pyrrole case radiative association was a minor channel, with an apparent rate constant of about 2.2×10^{-13} cm^3 $molecule^{-1}$ s^{-1}. Two major reaction products were observed, namely, the pyrrole molecular ion, corresponding to charge transfer, and the ion corresponding to vanadium ion addition with elimination of $H^\bullet$. Each of these latter channels had an apparent rate constant of about 9×10^{-10} cm^3 $molecule^{-1}$ s^{-1}. Since the direct charge-transfer channel for ground-state V^+ ions is endothermic by 33 kcal mol^{-1} and would certainly not be accessible to ground-state reactants, the presence of a major charge-transfer product suggests the presence of non-thermalized reactant ions (perhaps electronically excited ions, in view of the argon-cooling results noted below). However, this complex kinetic system was not fully characterized, and definitive conclusions are not justified. The observed rate of actual adduct formation gives a lower limit to the rate which would be observed in the absence of the competing reaction channels. The lower limit to the complex binding energy assigned in this way is 43 kcal mol^{-1}, but it is certain that the actual binding energy is considerably higher than this.

The reaction of pyrrole with Mo^+ yielded mainly RA adduct. There was a minor extent of other reaction channels in this system, which were not characterized.

W^+ was exceptional in its reactivity with pyrrole. Most (90%) of the numerous product ion peaks were distributed in the region between the W^+ peak and the $(W + \text{pyrrole})^+$ peak, indicating the occurrence of various elimination reactions. It did not seem useful to try to characterize this spectrum, which was additionally complicated by the overlapping of isotopic multiplets. Charge transfer and radiative association were both observed as minor channels, on the order of 5% each. Again, the small observed extent of adduct formation permitted assignment of a lower limit to the binding energy.

Ion Thermalization. A concern in metal-ion chemistry is the possibility of reactant ions possessing unrelaxed translational or electronic excitation. Some metal ions in the present study showed extensive ion−molecule elimination reactions or fast charge transfer which appeared likely to reflect the reactivity of uncooled reactant ions. To give more effective cooling of the initial ions and reduce or eliminate excited-reactant reaction pathways in these problematic cases, a cooling pulse of argon was introduced via a pulsed valve. Argon collisions are expected to be highly effective in relaxing excess translational energy of the reactant ions, while the effect on electronic excitation is hard to predict. The pressure of argon in the pulse was not characterized, so that the number of cooling collisions was not known directly, but the duration of the argon pulse was pushed up to a large enough value so that significant diffusional loss of ions from the cell was observed. This probably indicates hundreds of ion−argon collisions during the cooling pulse.

For the V^+ case, a few argon collisions were found to be effective in suppressing various minor elimination reactions, but even severe argon cooling brought about no significant change in the relative contributions of the three principal reaction products noted above. For Ti^+ and W^+ argon cooling made no important difference in the reactivity patterns described above. Collisional cooling should remove excess translational energy efficiently, so it can be suggested that the complex chemistry observed for these three ions was not attributable to initial unrelaxed translational energy of the reactants. The competing

TABLE 5: RA Kinetics Results and Binding Energies (BE; kcal mol^{-1}) for the Metal/Pyrrole Monomer Complexes

metal	k_{RA}(monomers)[a]	BE, StH	BE, VTST	BE, lit.	BE, DFT[h]
Na^+					25.8
Mg^+	0.066	40	43.9		36.0
Al^+	0.039	38	43.9		35.7
Si^+					64.8
Ti^+	1.8[b]				48.9
V^+	0.007[c]	>33[c,e]	>41[c,e]		49.4
Cr^+	0.045	39	42.5		41.4
Mn^+	0.066[d]	*d*	42.4[d]		37.4
Fe^+	1.0	53	54.1	48.3[f]	49.1
Co^+	13.0	>63[e]	>66[e]	59.8[g]	54.8
Ni^+	16.0	>64	>68		61.0
Cu^+	3.8	59	59		58.3
Mo^+	fast	>69[e]			38.6
W^+	~2.0[c]	>50[c,e]			58.8

[a] 10^{-10} cm^3 molecule^{-1} s^{-1}. [b] Rate constant for the association channel in the presence of N_2 bath gas (see the text). [c] Rate constant for the association channel only. Other competing reaction channels were much faster. The binding energy values for these metals are certainly substantially higher than the lower limits given here. See the text. [d] The high-pressure conditions for this measurement imply approximately 50% collisional association kinetics. StH provides no estimate of binding energy, and the VTST estimate is somewhat uncertain. [e] Lower limit binding energies taking into account a factor of 2 uncertainty in the rate constants. [f] Reference 33 (threshold CID). [g] Reference 34 (photodissociation threshold). [h] B3LYP−DFT calculations.

TABLE 6: RA Kinetics Results and Binding Energies (BE; kcal mol^{-1}) for the Metal/Pyrrole Dimer Complexes

metal	k_{RA}(dimer)	BE, StH	BE, VTST	BE, lit.	BE, DFT[d]
Na					19.6
Mg	<0.002[a]	<24[a]	<26.0[a]		18.7
Al	<0.002[a]	<24[a]	<25.2[a]		15.6
Cr	0.09	37	34.9		31.5
Mn	0.0007	*b*	27[b]		29.9
Fe	1.5	48	41.5		39.7
Co	6.6	55	46.4	48[c]	39.6
Ni	4.3	53	47.0		43.7
Cu	2.8	51	44.0		38.7
Mo	fast				
W	fast				

[a] No dimer complex was observed in these cases, so the rate constants and binding energy estimates for these two metals are only upper limits. [b] The high-pressure conditions for this measurement imply approximately 50% collisional association kinetics. StH provides no estimate of binding energy, and the VTST estimate is somewhat uncertain. [c] Reference 34 (photodissociation threshold). [d] B3LYP−DFT calculations.

reaction channels are presumably either true thermal-ion reactions or reactions of electronically excited metal ions.

RA Results. An illustrative plot of the sequential formation of copper complexes with one and two pyrrole molecules is shown in Figure 1. Table 5 shows the experimentally determined rate constants for monomer complexes, along with binding energies derived from these results by StH analysis and by VTST analysis, as well as binding energies calculated directly by B3LYP−DFT. Reactions of Ni^+, Co^+, and Mo^+ with pyrrole to form monomer complexes (Table 5) were fast, approaching the collisional limit. This allows us to give only lower-limit estimates of binding energies for these cases. Similarly, the reactions of the monomer complexes of Ni^+ and Co^+ to form dimer complexes (Table 6) were close enough to the collisional limits so that the binding energy estimates are very uncertain (and might also be regarded as lower limits).

A few literature values are also noted in the tables. The error bars on the experimental points in Figures 2−5 reflect the uncertainty corresponding to the estimated uncertainties in the rate constant determinations. There is the possibility of additional errors in these binding energy values associated with the kinetic modeling procedure, but there is no good basis for assigning these uncertainties.

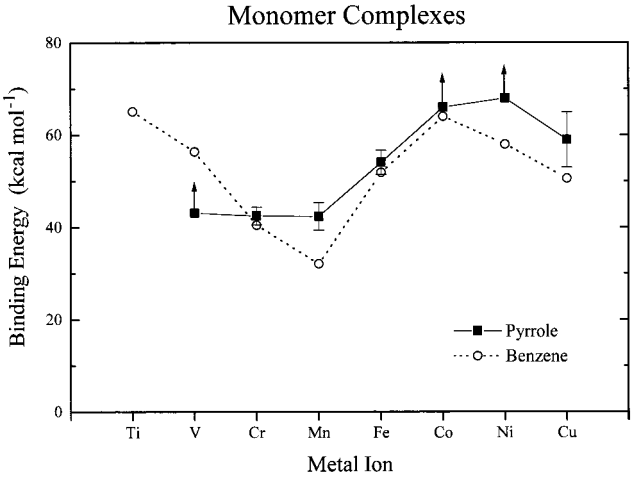

Figure 4. Binding energies of the first transition-metal row with benzene and pyrrole in monomer complexes. Note that the experimental value for V^+ is a lower limit because of competing reaction complications, and the actual value is definitely higher than shown. The Co^+ and Ni^+ points are also lower limits because of saturation, and the actual values may be higher. Benzene values from ref 32.

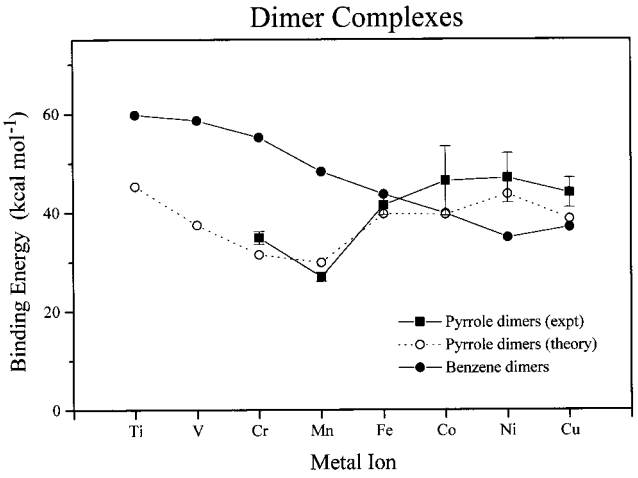

Figure 5. Binding energies of the first transition-metal row with benzene and pyrrole in dimer complexes. Benzene values from ref 32.

Table 6 shows rate constants for formation of dimer complexes (eq 4). The monomer complexes of pyrrole with Al^+ and Mg^+ did not react further to form dimer. Monomer complexes of Cr^+, Cu^+, Fe^+, Co^+, and Ni^+, as well as Mo^+ and W^+, reacted readily with a second pyrrole molecule, leading to dimer complexes. Surprisingly, formation of the dimer complex in the Mn^+ case was very slow, with a rate constant of 7×10^{-14} cm^3 molecule^{-1} s^{-1}, in contrast to the facile dimer formation for this metal ion with benzene (ref 32). With V^+ it was not possible to tell whether dimer complex was formed, because of the low abundance of monomer complex reactant.

As an indication of the nature of the observed dimer complexes, collision-induced dissociation of the Co^+/pyrrole dimer complex was carried out with pyrrole as the bath gas. The only CID product was the monomer complex $Co(C_4H_5N)^+$, suggesting that the pyrrole molecule is bound as an intact entity.

The results presented in Table 6 are based on a free rotor treatment of the lowest vibrational frequency of the dimer in

TABLE 7: Ligand Exchange Equilibrium at 300 K[a]

metal	$[MPy^+]/[MBz^+]$	$K_{equilib}$	$\Delta G°$ [b]	$\Delta H°$ [b,c]
Mg^+	5.5	8.7×10^3	5.4	5.4
Al^+	22	3.5×10^4	6.2	6.2

[a] Pyrrole pressure 1.2×10^{-9} Torr, benzene pressure 2×10^{-6} Torr. [b] Derived thermochemical value (kcal mol^{-1}) for transfer of M^+ from pyrrole to benzene. [c] Assuming $\Delta S° = 0$.

the VTST analysis. The dimer binding energies would be 1.2, 0.9, 2.1, 3.1, 3.6, and 1.4 kcal/mol higher for the Cr, Mn, Fe, Co, Ni, and Cu dimers if this mode had instead been treated as a harmonic vibration.

Ligand Exchange Equilibrium Results. The ligand exchange competition between benzene and pyrrole was measured for Mg^+ and for Al^+, with the results shown in Table 7. The values of $\Delta G°$ for transferring the metal ion from one ligand to the other are obtained directly, but since temperature-dependent data were not obtained, the extraction of $\Delta H°$ from the data requires an estimate of $\Delta S°$. $\Delta S°$ was taken to be zero, on the basis of the assumptions that the 6-fold rotational symmetry of benzene is retained in the two complexes, and that the vibrational, rotational, and translational contributions to the ligand exchange entropy are small.

Discussion

Binding Sites and Geometries. All of the information we have about the binding geometries comes from the quantum chemistry results. The metals all bind preferentially at a π site lying over the ring. Table 1 shows the optimized metal-ion positions over the ring, as well as the ring−metal distance. The metal ion never favors the nitrogen side of the ring, but there is considerable variability in how far it is displaced in the direction away from the nitrogen. For instance, the calculations suggest that Ti^+ and Co^+ lie nearly over the center of the ring, while Cr^+ and Cu^+ (as well as the larger metals Mo^+ and W^+) are so far displaced that they lie outside the perimeter of the carbon skeleton of the ring. We have no clear rationalization for these geometry variations.

The accumulation of positive charge in the nitrogen region of this ring system gives strong electrostatic inhibition to binding a metal ion directly to the nitrogen center. In these calculations, only the Cu^+ ion was found to have a possible nitrogen binding site in addition to its normal π site. A local potential minimum or inflection point was found with the Cu^+ essentially directly above the nitrogen, apparently interacting with the p_z orbital of the nitrogen atom. This site was 16 kcal higher in energy than the π site. It had one near-zero vibrational frequency (-1.9 cm^{-1}), suggesting that it is a very shallow well, but the barrier to the metal ion moving over to the π binding site was not investigated.

Comparison with Literature Binding Energies. Only a few binding energies of metal ions to pyrrole have been reported for comparison with the present results. Jacobson's group looked at the Fe^+ case using threshold CID,[33] and Freiser's group studied Co^+ monomers and dimers by photodissociation threshold measurements.[34] The present experimental value for the Fe^+ monomer complex is about 6 kcal mol^{-1} higher than that of Bakhtiar and Jacobson,[33] which is not unreasonable given the uncertainties of both techniques, while the present DFT-calculated value is in excellent agreement with their measurement. The Co^+ monomer complex shows fair agreement between the literature and the present calculated value, as indicated in Table 5. The present lower limit on this value from RA kinetics is, as discussed below, higher for reasons that are not clear. The 48 kcal mol^{-1} binding energy of Nanayakkara et al.[34] for $Co(Py)^+-Py$ is in accord with the present value of 46 kcal mol^{-1}, while both of these measurements are substantially higher than the DFT result.

Comparison of Different Modeling Approaches. The data were analyzed by the semiquantitative StH estimation approach, as well as by detailed VTST modeling. The comparison offers some guidance to how much confidence to place in the StH modeling approach. (Note that such comparisons do not address the question of the accuracy of the RA kinetics approach to determining binding energies, but only assess how faithfully the StH scheme approximates the results of accurate kinetic modeling within the transition-state theory framework for interpreting RA kinetics data.) The comparisons displayed in Tables 5 and 6 show the expected semiquantitative agreement, with deviations of a few kilocalories per mole. This adds weight to previous comparisons[9,27,35] suggesting that the StH approach is a useful semiquantitative guide within an uncertainty of a few kilocalories per mole.

Binding Energies for Benzene and Pyrrole Complexes. Benzene often serves as a model compound in studies of metal-ion interactions with aromatic compounds. The first-row transition-metal ions form monomer complexes as well as dimers with benzene.[32] As can be seen in Figure 4, a similar trend in binding energies is observed for benzene and pyrrole monomer complexes across the first transition-metal row. The dip at Cr^+/Mn^+ in both cases is striking, and is well understood in terms of the d orbital contributions to binding.[32]

On the other hand, there is a strong contrast between the binding energy patterns for the dimer complexes (Figure 5). The low second-ligand pyrrole binding energy for Mn^+, with a sharp rise in going from Mn^+ to Fe^+, parallels the similar pattern in the corresponding first-ligand binding energies with pyrrole (Figure 4). As shown in Figure 5, however, this pattern was not seen in the benzene dimer complex results of Meyer and Armentrout,[32] which showed a steady modest drop in going from Cr^+ across to Co^+.

The RA kinetics results for Co^+ and Ni^+ monomer complexes (and to a lesser extent the dimer complexes as well) are unexpected and somewhat puzzling. As displayed clearly in Figure 2, the very efficient association reactions of these two metal ions imply lower limits to the binding energies which are rather far above the calculated values for the π complexes. Even though the binding for these two ions is expected to be quite strong, this discrepancy is uncomfortably large. As discussed above, the possibility of rearrangement to a pyrrole-nine structure was considered, but was not supported by calculations. There is the possibility that these ions form complexes with an as-yet unconsidered highly stable rearranged structure, such as a metal-insertion structure. These possibilities will need further investigation. A similar problem exists for Mo^+, although in this case the quantum-chemical calculations are much less confident.

For the nontransition metals, the present ligand-transfer equilibrium experiments, giving the results shown in Table 7, give an especially satisfactory comparison between benzene and pyrrole. Another source of information on this question for Al^+ is a recent RA kinetics study,[23] reporting a measurement very comparable to the present RA kinetics work, which assigned a benzene value of 35.2 ± 2 kcal mol^{-1}. Moreover, a B3LYP−DFT calculation similar to the present ones gave an Al^+/benzene binding energy of 29.3 kcal mol^{-1}. We can thus compare three independent ways to estimate the increase of Al^+ binding energy to pyrrole relative to benzene: (a) Comparing direct RA kinetics

values gives an increment of 9 kcal mol^{-1}. (b) The present ligand exchange equilibrium gives an increment of 6.2 kcal mol^{-1}. (c) Comparison of DFT calculations gives an increment of 6.4 kcal mol^{-1}. Overall, this incremental energy can be assigned with considerable confidence in the vicinity of 7 ± 2 kcal mol^{-1}. Note that all three of these difference determinations versus benzene are independent of the correctness of the absolute binding energies.

The situation with Mg^+ is similar. Radiative association with benzene was observed[36] to have a rate constant of 4.5×10^{-12} cm^3 molecule^{-1} s^{-1}, which is 2.6 times faster than reported for Al^+.[23] This would indicate an RA kinetics-derived binding energy with benzene about 2 kcal mol^{-1} higher than for Al^+, or 37 kcal mol^{-1}. We can again compare three independent estimates of the Mg^+ binding energy increment in going from benzene to pyrrole: (a) Comparing direct RA kinetics values gives an increment of 7 kcal mol^{-1}. (b) The present ligand exchange equilibrium gives an increment of 5.4 kcal mol^{-1}. (c) The present DFT results give an increment of 6.1 kcal mol^{-1}. This Mg^+ incremental energy appears to be similar to or slightly less than for Al^+, in the vicinity of 6 ± 2 kcal mol^{-1}.

Mg^+ and Al^+ binding to π systems is largely due to electrostatic and polarization factors. It is thus natural that the charge−dipole interaction in the pyrrole complexes would give the observed enhancement of the binding energies relative to benzene. Binding to transition-metal ions is more complicated, and seems to give a less regular comparison between benzene and pyrrole.

Monomer vs Dimer Complexes. Comparing Tables 5 and 6, it is seen that the binding of the second pyrrole ligand is consistently weaker than binding of the first. For Mg^+ and Al^+ no dimer complex was observed at the limit of the experiments, which parallels the similar situation for benzene. Similarly for the late transition metals, the dimer binding energies reported by Meyer and Armentrout[32] for benzene are also weaker than the monomer binding energies. On the other hand, they reported the Cr^+ and Mn^+ dimer binding to be stronger than the monomer binding, which is an interesting contrast to pyrrole.

A direct comparison is useful between the present Cr^+/pyrrole observations and the Cr^+/benzene results of Lin and Dunbar[28] by the same technique. Rate constants of 0.18×10^{-10} and 2.3×10^{-10} cm^3 molecule^{-1} s^{-1} were reported by the latter for the benzene monomer and dimer association rate constants, respectively, compared with the present values of 0.045×10^{-10} and 0.09×10^{-10} for pyrrole. Given equal binding energies, the association rate constants for the smaller pyrrole system would be expected to be about 4 times slower than the benzene system, which is close to the actually observed values, leading to our assignment of similar Cr^+ binding energies for benzene and pyrrole as reflected in Figures 4 and 5. Our assignments here give the pyrrole monomer as more strongly bound than the dimer, while the reverse was true for the benzene assignments in refs 28 and 32.

Calculated Binding Energies. The B3LYP−DFT calculations gave absolute and relative binding energies for the monomer and dimer complexes. As Figures 2 and 3 show, the calculated pattern of relative binding energies tracks the corresponding pattern of experimental results quite closely, giving support to the validity of both sets of values.

As is shown clearly in Figure 2 for the transition metals, and is also seen for Mg^+ and Al^+ in Table 5, the absolute calculated monomer values are generally a few kilocalories per mole lower than the experimental numbers. To give further context for this observation, we can note a study by Stöckigt indicating that the absolute binding energies of Al^+ with various ligands calculated by B3LYP−DFT were systematically low by about 5 kcal mol^{-1} relative to high-level, large-basis ab initio results.[37] A more recent report[38] confirms that B3LYP−DFT tends to give relatively low binding energies for Al^+/pyrrole compared with various other computational approaches. This latter study gives a G2MP2 binding energy of 40.9 kcal mol^{-1} for Al^+/pyrrole, which approaches the best currently feasible computational level. This is several kcal/mol higher than the value calculated here, but is in reasonable agreement with the present experimental result. Thus, there is reason to suspect that B3LYP−DFT binding energies may be a few kcal/mol low for this system, and (even more speculatively) perhaps for other systems considered in the present work. However, there is also reason to suspect that the RA kinetics analysis might be systematically too high for these metal-ion/π complexes, since the binding energy of Cr^+/benzene obtained by a similar RA kinetics analysis appears to be 3−4 kcal mol^{-1} too high.[20] Also supporting the validity of the B3LYP−DFT approach are recent experimental determinations of Na^+ binding energies to benzene[39,40] which do not show large systematic deviations relative to DFT calculations. In any case it is clear that uncertainties of several kcal/mol are appropriate to absolute binding energy values from either RA kinetics analysis or DFT calculations at the present level.

We have confidence that the present results accurately reflect the trends of pyrrole binding energies across the range of metal ions studied. The assignment of the absolute binding energy scale within a range of about 5 kcal mol^{-1} is not yet settled to our satisfaction, and is the subject of continuing investigation.

Conclusions

The trend of pyrrole binding energies across the transition-metal ion series is displayed unequivocally by both the experimental and the computational results. In a quite close parallel to the trend of the corresponding benzene values reported by Armentrout's group,[32] we find that the pyrrole binding energies to transition-metal ions decrease from V^+ down to a minimum at Cr^+/Mn^+, followed by a strong rise toward Co^+ and Ni^+, with a final drop-off at Cu^+. This confirms that π binding to pyrrole and to benzene is highly comparable, and is governed by similar electronic interaction effects.

Experiment and theory both indicate that binding to pyrrole is stronger than binding to benzene for Mg^+ and Al^+ by 6−7 kcal mol^{-1}. This is rationalized on the basis that the dipolar attractive interaction enhances electrostatic binding to pyrrole relative to benzene. The comparison of pyrrole and benzene is less clear for the transition-metal ions, where electronic binding effects are larger and more complicated.

The calculations give no encouragement to the possibility of a lone pair site, or alternatively a tetrahedral sp^3 site, for metal-cation binding to the pyrrole nitrogen. Although there is the indication of an incipient local potential well at the nitrogen site for at least some metals, notably Cu^+, the calculations indicate that the destabilizing electrostatic effect of the dipolar charge distribution rules out formation of a stable binding site at nitrogen for any of the metal ions.

The present results give pyrrole binding thermochemistry for the monomers relative to the corresponding benzene complexes with satisfactory consistency and confidence. The experimental RA kinetics monomer binding energies are higher than the B3LYP−DFT-calculated ones by varying amounts, although in one case, Al^+/pyrrole, a recent G2MP2 calculation is in much better agreement with our experimental number. For these

systems it is suspected that either the calculations are consistently too low or the RA kinetics results are too high by a few kilocalories per mole, and until further evidence accumulates we would be cautious about assigning the absolute scale of binding energies in this set of complexes better than a range of perhaps 5 kcal mol^{-1} uncertainty.

For the dimer complexes, experimental and calculated binding energies are in satisfactory agreement, giving confidence in both the trend and the absolute values from the present results. The dimer binding energies for the late transition metals are generally not very different from those reported for benzene by Armentrout's group, but Mn^+ and Cr^+ (as well as the calculated values for the earlier transition metals) are in striking contrast to the benzene values, being lower by an amount on the order of 20 kcal mol^{-1}.

Acknowledgment. The support of the National Science Foundation (S.J.K.) and of the donors of the Petroleum Research Fund, administered by the American Chemical Society (S.J.K. and R.C.D.) is gratefully acknowledged. We thank the reviewer who drew our attention to the possibility of rearrangements to a pyrrolenine structure for the complexes.

References and Notes

(1) Lewis, F. D.; Yang, J. S.; Stern, C. L. *J. Am. Chem. Soc.* **1996**, *118*, 2772.
(2) Boone, B. J.; Klein, D. P.; Seyle, J. W.; Mendez, N. Q.; Arif, A. M.; Gladysz, J. A. *J. Am. Chem. Soc.* **1996**, *118*, 2411.
(3) Wilson, M. A.; Pohorille, A. *J. Am. Chem. Soc.* **1996**, *118*, 6580.
(4) Ma, J. C.; Dougherty, D. A. *Chem. Rev.* **1997**, *97*, 1303.
(5) Ryzhov, V.; Dunbar, R. C. *J. Am. Chem. Soc.* **1999**, *121*, 2259.
(6) Dunbar, R. C. *J. Phys. Chem. A* **1998**, *102*, 8946.
(7) Mecozzi, S.; West, A. P., Jr.; Dougherty, D. A. *J. Am. Chem. Soc.* **1996**, *118*, 2307.
(8) Mecozzi, S.; West, A. P. Jr.; Dougherty, D. A. *Proc. Natl. Acad. Sci. U.S.A.* **1996**, *93*, 10566.
(9) Dunbar, R. C. *Int. J. Mass Spectrom. Ion Processes* **1997**, *160*, 1.
(10) Klippenstein, S. J.; Yang, Y.-C.; Ryzhov, V.; Dunbar, R. C. *J. Chem. Phys.* **1996**, *104*, 4502.
(11) Uppal, J. S.; Staley, R. H. *J. Am. Chem. Soc.* **1982**, *104*, 1235.
(12) Ryzhov, V.; Yang, C.-N.; Klippenstein, S. J.; Dunbar, R. C. *Int. J. Mass Spectrom.* **1999**, *185*−*187*, 913.
(13) Bartmess, J. E.; Georgiadis, R. M. *Vacuum* **1983**, *33*, 149.
(14) Becke, A. D. *J. Chem. Phys.* **1993**, *98*, 5648.
(15) GAUSSIAN 94: Frisch, M. J.; Trucks, G. W.; Schlegel, H. B.; Gill, P. M. W.; Johnson, B. G.; Robb, M. A.; Cheeseman, J. R.; Keith, T.; Petersson, G. A.; Montgomery, J. A.; Raghavachari, K.; Al-Laham, M. A.; Zakrzewski, V. G.; Ortiz, J. V.; Foresman, J. B.; Cioslowski, J.; Stefanov, B. B.; Nanayakkara, A.; Challacombe, M.; Peng, C. Y.; Ayala, P. Y.; Chen, W.; Wong, M. W.; Andres, J. L.; Replogle, E. S.; Gomperts, R.; Martin, R. L.; Fox, D. J.; Binkley, J. S.; Defrees, D. J.; Baker, J.; Stewart, J. P.; Head-Gordon, M.; Gonzalez, C.; Pople, J. A., Gaussian, Inc., Pittsburgh, PA, 1995.
(16) Xantheas, S. S. *J. Chem. Phys.* **1996**, *104*, 8821.
(17) Moore, C. E. *Atomic Energy Levels; As Derived from the Analysis of Optical Spectra*}; U.S. National Bureau of Standards (U.S.) Circular No. 467; Vol. I, 1949; Vol. II, 1952.
(18) Bauschlicher, C. W.; Partridge, H.; Langhoff, S. R. *J. Phys. Chem.* **1992**, *96*, 3273.
(19) Klippenstein, S. J. Unpublished results.
(20) Yang, C.-N.; Klippenstein, S. J. *J. Phys. Chem. A* **1999**, *103*, 1094.
(21) Dunbar, R. C. Review: Ion−Molecule Radiative Association. In *Current Topics in Ion Chemistry and Physics*; Ng, C. Y., Baer, T., Powis, I., Eds.; Wiley: New York, 1994; Vol. II.
(22) Dunbar, R. C. New Approaches to Ion Thermochemistry via Dissociation and Association. In *Advances in Gas-Phase Ion Chemistry*; Babcock, L. M., Adams, N. G., Eds.; JAI Press: Greenwich, CT, 1996; Vol. 2, p 87.
(23) Dunbar, R. C.; Klippenstein, S. J.; Hrušàk, J.; Stöckigt, D.; Schwarz, H. *J. Am. Chem. Soc.* **1996**, *118*, 5277.
(24) Cheng, Y. W.; Dunbar, R. C. *J. Phys. Chem.* **1995**, *99*, 10802.
(25) Weddle, G. H.; Dunbar, R. C. *Int. J. Mass Spectrom. Ion Processes* **1994**, *134*, 73.
(26) Ryzhov, V.; Yang, Y.-C.; Klippenstein, S. J.; Dunbar, R. C. *J. Phys. Chem. A* **1998**, *102*, 8865.
(27) Ryzhov, V.; Dunbar, R. C. *Int. J. Mass Spectrom. Ion Processes* **1997**, *167/168*, 627−635.
(28) Lin, C.-Y.; Dunbar, R. C. *Organometallics* **1997**, *16*, 2691.
(29) Klippenstein, S. J.; Wagner, A. F.; Dunbar, R. C.; Wardlaw, D. M.; Robertson, S. H.; Diau, E. W. VariFlex computer code, available via anonymous FTP from london.tcg.anl.gov.
(30) Su, T.; Chesnavich, W. J. *J. Chem. Phys.* **1982**, *76*, 5183.
(31) Nguyen, V. Q.; Turecek, F. *J. Mass Spectrom.* **1996**, *31*, 1173.
(32) Meyer, F.; Khan, F. A.; Armentrout, P. B. *J. Am. Chem. Soc.* **1995**, *117*, 9740.
(33) Bakhtiar, R.; Jacobson, D. B. *J. Am. Soc. Mass Spectrom.* **1996**, *7*, 938.
(34) Nanayakkara, V. K.; Freiser, B. S. *J. Mass Spectrom.* **1997**, *32*, 475.
(35) Dunbar, R. C. *Int. J. Mass Spectrom. Ion Processes* **1990**, *100*, 423.
(36) Ryzhov, R. V. Ph.D. Thesis, Case Western Reserve University, Cleveland, OH, 1998.
(37) Stöckigt, D. *J. Phys. Chem. A* **1997**, *101*, 3800.
(38) Stöckigt, D. *Organometallics* **1999**, *18*, 1050.
(39) Hoyau, S.; Norrman, K.; McMahon, T.; Ohanessian, G. *J. Am. Chem. Soc.* **1999**, *121*, 8864.
(40) Armentrout, P. B.; Rodgers, M. T. *J. Phys. Chem. A*, in press.